Article

Sustainable methane utilization technology via photocatalytic halogenation with alkali halides

Jun Ma [1,2,3,10], Can Zhu [4,10], Keke Mao [5,10], Wenbin Jiang[1], Jingxiang Low[1], Delong Duan[1], Huanxin Ju [6], Dong Liu [1,2], Kun Wang[4], Yijing Zang[7,8], Shuangming Chen [1], Hui Zhang [8], Zeming Qi[1], Ran Long [1] ✉, Zhi Liu [7,8], Li Song [1] & Yujie Xiong [1,3,9] ✉

Methyl halides are versatile platform molecules, which have been widely adopted as precursors for producing value-added chemicals and fuels. Despite their high importance, the green and economical synthesis of the methyl halides remains challenging. Here we demonstrate sustainable and efficient photocatalytic methane halogenation for methyl halide production over copper-doped titania using alkali halides as a widely available and non-corrosive halogenation agent. This approach affords a methyl halide production rate of up to 0.61 mmol h^{-1} m^{-2} for chloromethane or 1.08 mmol h^{-1} m^{-2} for bromomethane with a stability of 28 h, which are further proven transformable to methanol and pharmaceutical intermediates. Furthermore, we demonstrate that such a reaction can also operate solely using seawater and methane as resources, showing its high practicability as general technology for offshore methane exploitation. This work opens an avenue for the sustainable utilization of methane from various resources and toward designated applications.

Methyl halides, such as chloromethane (CH$_3$Cl) and bromomethane (CH$_3$Br), represent versatile platform molecules for producing various value-added chemicals and fuels (e.g., light olefins, pharmaceutical intermediates and organoboron agents)[1–4]. Industrially, the production of methyl halides primarily involves methanol as feedstock, which is also precious fuel and chemical, along with complicated process and intensive energy input, inducing high capital cost (Supplementary Fig. 1a)[5,6]. Against this background, methane (CH$_4$), whose reserves have

been recently bloomed due to the exploration of methane hydrate, shale gas and coalbed methane, has emerged as a potential substitution of methanol as carbon feedstock for methyl halide production[7–12]. Specifically, Olah and coworkers pioneeringly reported the possibility of catalytic methane halogenation for methyl halide production, paving a way for cheap and effective production of methyl halides[13].

Since then, a series of important advances have been achieved in methane halogenation, pushing forward its development toward

[1]School of Chemistry and Materials Science, National Synchrotron Radiation Laboratory, School of Nuclear Science and Technology, University of Science and Technology of China, 230026 Hefei, Anhui, China. [2]Suzhou Institute for Advanced Research, University of Science and Technology of China, 215123 Suzhou, Jiangsu, China. [3]Institute of Energy, Hefei Comprehensive National Science Center, 350 Shushanhu Rd., 230031 Hefei, Anhui, China. [4]Department of Chemistry, Fudan University, 2005 Songhu Road, 200438 Shanghai, Yangpu District, China. [5]School of Energy and Environment Science, Anhui University of Technology, 243032 Maanshan, Anhui, China. [6]PHI China Analytical Laboratory, CoreTech Integrated Limited, 402 Yinfu Road, 211102 Nanjing, Jiangsu, China. [7]School of Physical Science and Technology, ShanghaiTech University, 201203 Shanghai, China. [8]State Key Laboratory of Functional Materials for Informatics, Shanghai Institute of Microsystem and Information Technology, Chinese Academy of Sciences, 200050 Shanghai, China. [9]Anhui Engineering Research Center of Carbon Neutrality, College of Chemistry and Materials Science, Key Laboratory of Functional Molecular Solids, Ministry of Education, Anhui Normal University, 241002 Wuhu, Anhui, China. [10]These authors contributed equally: Jun Ma, Can Zhu, Keke Mao. ✉e-mail: longran@ustc.edu.cn; yjxiong@ustc.edu.cn

practical applications[1,3,14–17]. For example, Zhang and coworkers employed FePO$_4$/SiO$_2$ for oxybromination of methane at 570 °C using HBr as halogen agent, which achieved a methane conversion of 50% and a selectivity of 48% for CH$_3$Br production[18]. Photochemical technology was also employed in methane halogenation using halide under UV irradiation (Supplementary Fig. 1b)[19–21]. Notwithstanding its rapid advancement, there are still critical limitations (e.g., corrosive feed gas, high working temperature and unsatisfactory selectivity) which defer the methane halogenation toward substituting the conventional industrial methyl halide production[22,23]. The decisive limitation is the involvement of dangerous feed gas (e.g., Cl$_2$, HCl, and HBr) in the reaction, which can lead to potential hazards and corrosion of catalysts and reactors. Therefore, it is an urgent task to develop safe and sustainable approaches for methane halogenation using widely available halogen sources.

Alkali halides, especially sodium halide, represent a class of green and cheap halogen sources, yet their inertness greatly hinder their utilization in methane halogenation. Although a previous report suggested that the methane chlorination with metal chlorides may be achieved by UV-responsive photocatalyst, the reported case only exhibited low product selectivity and catalyst durability, and as such, the products can hardly be continuously converted into value-added chemicals and fuels[18]. Here, we present a simple yet effective photocatalytic route for activating alkali halides, and utilize alkali halides as halogen source for methane halogenation. Specifically, the Cu-doped porous TiO$_2$ photocatalyst (Cu–TiO$_2$) is employed to drive the methane halogenation under moderate conditions (i.e., room temperature and ambient pressure) (Fig. 1 and Supplementary Fig. 1c). We adopt the photocatalytic methane chlorination as a proof-of-concept example using sodium chloride as halogen agent, achieving a methyl chloride production rate of 0.61 mmol h^{-1} m^{-2} with a selectivity of 83.7% upon light irradiation. In situ spectroscopic characterizations and theoretical simulations manifest that the methane molecule can be first dissociated into methyl intermediate on the surface of the photocatalyst. In addition, evidenced by ambient pressure X-ray photoelectron spectroscopy (AP-XPS), the halogen ions (i.e., chloride in this case) from alkali halides can be oxidized and activated by photogenerated holes from the photocatalyst to form active chloride species. As such, the produced active chloride species can react with the methyl intermediates to produce methyl chloride. This approach enables the direct use of seawater and methane feedstocks for methyl chloride production, largely extending its practical applications such as offshore methane exploitation. Moreover, we construct reaction systems for production of methanol and pharmaceutical intermediates (i.e., methyl o-toluate and 1-methylindole) via a methyl halide mediated pathway. This work provides an approach for selective methane halogenation under mild conditions using green and cheap alkali halide as halogen source, shedding significant light on sustainable methyl halide production.

Results

Catalyst synthesis and characterization

In this work, the Cu, which has been proven to play a critical role as active sites for methane activation on particulate methane monooxygenase in nature, is selected to dope TiO$_2$ photocatalysts for methane halogenation[15,22]. The Cu-doped porous TiO$_2$ nanostructures (denoted as X%Cu–TiO$_2$, where X represents the molar percentage of Cu atoms in precursors) are synthesized in gram-scale via a simple sol–gel process (Supplementary Fig. 2a). Transmission electron microscopy (TEM) images (Supplementary Figs. 2b, c, 3) reveal the porous morphology of as-synthesized samples. As determined by nitrogen adsorption–desorption isotherms, all the prepared samples exhibit large specific surface area with a pore size distribution of ca. 10 nm (Supplementary Fig. 4 and Table 1), endowing enormous active sites for photocatalytic reaction.

Energy-dispersive X-ray spectroscopy (EDS) mapping suggests the presence of Ti, O and Cu elements (Supplementary Fig. 2d), affirming the composition of the prepared samples. According to powder X-ray diffraction (XRD) characterization (Supplementary Fig. 2e), the crystal phase of TiO$_2$ maintains unchanged after introduction of Cu elements. In addition, as revealed by UV–vis–NIR diffuse reflectance spectroscopy (Supplementary Fig. 5), the light absorption edges of the X%Cu–TiO$_2$ red shift with the increasing Cu concentration due to the presence of oxygen vacancies (V_O) (Supplementary Fig. 6) and $2E_g \rightarrow 2T_{2g}$ transitions from O to Cu atoms[24]. Moreover, the enhanced absorptions of the samples in the visible–near-infrared regions are attributed to the d–d transitions of the Cu dopants[24]. Synchrotron-radiation photoemission spectroscopy (SRPES) indicates that the valence-band maxima (VBM) of 0%Cu–TiO$_2$ and 2%Cu–TiO$_2$ are 3.56 and 3.46 eV below the Fermi level (E_F), respectively (Supplementary Fig. 7). Combined with the determined band gaps from light absorption spectra (Supplementary Fig. 8), the band structure changes of TiO$_2$ before and after Cu-doping can be estimated, showing that the Cu-doping can slightly shift both the VBM and conduction band minimum (CBM) of TiO$_2$ (Supplementary Fig. 9). Furthermore, X-ray photoelectron spectroscopy (XPS), X-ray absorption spectroscopy (XAS) and X-ray absorption fine structure (XAFS) spectroscopy confirm that the Cu is doped into the TiO$_2$ matrix as a single-site substitution and exhibits a +2 oxidation state in 2%Cu–TiO$_2$ (Supplementary Figs. 10–12). Furthermore, the Fourier-transformed (FT) Ti K-edge extended XAFS (EXAFS) spectra of the 0%Cu–TiO$_2$ and 2%Cu–TiO$_2$ demonstrate that the Ti–O coordination numbers of TiO$_2$
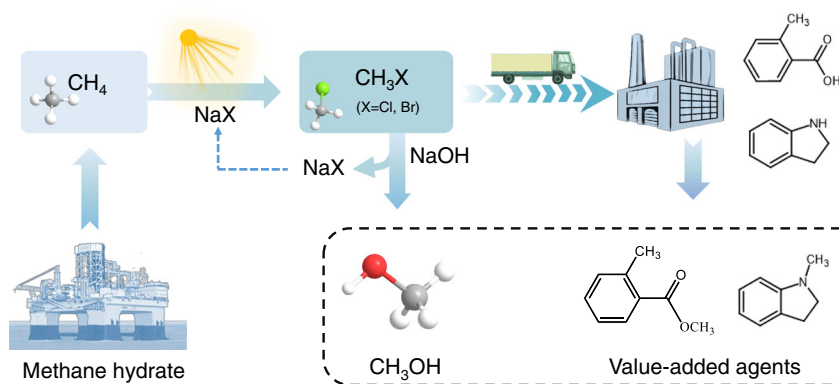

Fig. 1 | Schematic illustration for the proposed concept. The photocatalytic methane halogenation using alkali halide as a halogenation agent at room temperature, and the successive transformations into fuels and chemicals.
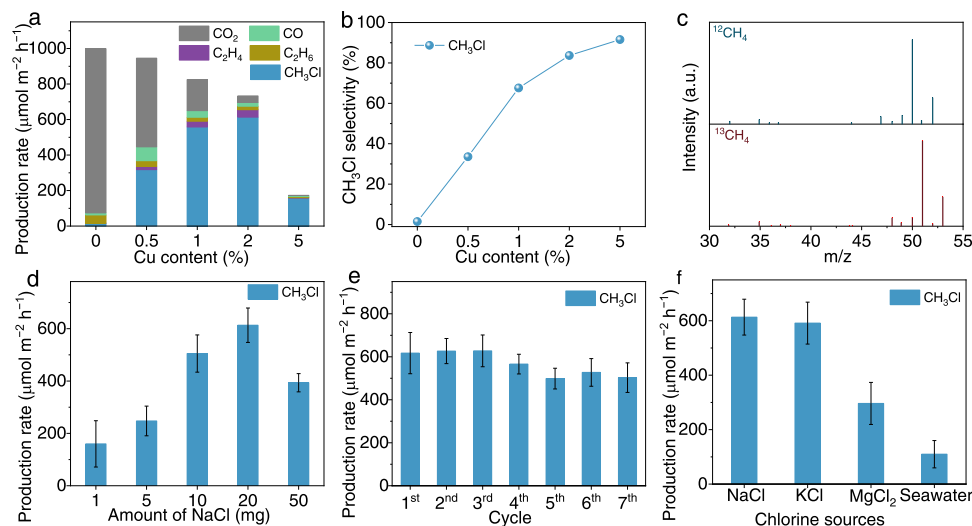
Fig. 2 | Photocatalytic halogenation of CH_4 under different conditions. **a**, **b** Photocatalytic methane halogenation efficiency (**a**) and selectivity (**b**) of $X\%$ Cu–TiO$_2$ toward CH_3Cl production. **c** Mass spectra of $^{12}CH_3Cl$ ($m/z = 50$) and $^{13}CH_3Cl$ ($m/z = 51$) produced over 2%Cu–TiO$_2$ via photocatalytic methane halogenation. **d** Production rates of CH_3Cl via photocatalytic methane halogenation over 2% Cu–TiO$_2$ with different amounts of NaCl. **e** The cyclic test of photocatalytic CH_3Cl production over 2%Cu–TiO$_2$. **f** Photocatalytic production rates of CH_3Cl via methane halogenation over 2%Cu–TiO$_2$ using various chlorine sources. The light intensity is 600 mW cm^{-2} for all the measurements here. Error bars indicate standard deviations.

decrease from 3.98 to 3.08 after Cu doping (Supplementary Fig. 2f, g and Supplementary Tables 2, 3), suggesting the existence of oxygen vacancies. This result collaborates that the Cu-doping can induce the formation of oxygen vacancies on the TiO$_2$.

Photocatalytic performance

After recognizing the physicochemical properties of prepared samples, we are now in a position to evaluate their applicability in photocatalytic methane halogenation. The photocatalytic experiments are carried out through a gas-solid phase reaction using sodium halide (e.g., NaCl and NaBr) as halogen agent at ambient conditions (Supplementary Figs. 13, 14). The test is first performed by varying doping parameters to screen optimal photocatalysts under the light illumination of 600 mW cm^{-2}. As shown in Fig. 2a and Supplementary Fig. 15, the 0%Cu–TiO$_2$ shows negligible CH_3Cl production, while the CH_3Cl production rate gradually increases with the increase of Cu content from 0.5 to 2%, suggesting the important role of Cu dopants in triggering methane halogenation. Specifically, the 2%Cu–TiO$_2$ achieves a methyl chloride production rate of 0.61 mmol h^{-1} m^{-2} with a selectivity of 83.7%. Yet, the overdose of Cu dopants (5%Cu–TiO$_2$) can lead to photogenerated charge recombination[25], resulting in decrease in CH_3Cl production rate. The selectivities toward the CH_3Cl production of the prepared samples shown in Fig. 2b imply the strong correlation of the CH_3Cl production with Cu contents, further confirming the critical role of Cu in such a reaction (Supplementary Fig. 16). The performance of photocatalytic methane chlorination over CuO-loaded TiO$_2$ nanostructures is far lower than that of the Cu–TiO$_2$ (Supplementary Fig. 17), indicating the significant role of Cu doping in methane and halide activation that induces oxygen vacancies with localized charge trapping centers on TiO$_2$. Moreover, the apparent quantum efficiency (AQE) over 2%Cu–TiO$_2$ is measured to be 5.4% at 254 nm and 0.3% at 365 nm monochromatic light irradiation. To clarify the accuracy of our obtained results, we conduct the isotope labeling test using $^{12}CH_4$ or $^{13}CH_4$ as the feed gas to perform photocatalytic halogenation of CH_4 over 2%Cu–TiO$_2$ (Fig. 2c). The location of the strongest peak changes from $m/z = 50$ (using $^{12}CH_4$ as fed gas) to $m/z = 51$ (using $^{13}CH_4$ as fed gas), verifying that the carbon source of generated CH_3Cl indeed originates from CH_4.

Upon identifying the optimal photocatalyst, we evaluate the influence of experimental parameters on the photocatalytic methane

halogenation performance of the optimized sample (i.e., 2%Cu–TiO$_2$). As revealed in Fig. 2d, the 20 mg is the optimal loading content of the NaCl in the system. The overloading of NaCl (i.e., 50 mg) can lead to the decrease in the photocatalytic methane halogenation performance due to the occupied surface active sites on the photocatalyst by the NaCl. In addition, it is unveiled that the high intensity of light irradiation is beneficial for optimizing the photocatalytic methane halogenation, elevating the methyl chloride production rate up to 0.69 mmol h^{-1} m^{-2} at 800 mW cm^{-2} (Supplementary Fig. 18a). It is worth mentioning that the Cu–TiO$_2$ catalyst can drive photocatalytic halogenation of methane under visible light irradiation (Supplementary Fig. 18b). Moreover, we have performed a time-dependent measurement with the continued light irradiation up to 14 h. As shown in Supplementary Fig. 19, the CH_3Cl production gradually increases and then becomes steady with the evolution of reaction time. In the meantime, the amount of H$_2$, generated during photocatalytic methane chlorination, is nonstoichiometric to the amount of methyl chloride (Supplementary Fig. 20), which results from probable consumption of lattice oxygen in TiO$_2$ during photocatalytic CH_4 chlorination. The recovery of consumed lattice oxygen can be easily conducted in the air to regenerate the pristine structure of Cu–TiO$_2$. Interestingly, the production rate of CH_3Cl obviously decreases to 0.44 mmol h^{-1} m^{-2} along with negligible H$_2$ production (Supplementary Fig. 21a) when the photocatalytic methane halogenation is performed in the absence of H$_2$O. In addition, the CH_3Cl production gradually becomes steady at about 8 h (Supplementary Fig. 21b), indicating the significant role of H$_2$O in photocatalytic methane halogenation reaction over Cu–TiO$_2$ catalyst.

The practical applicability of the Cu–TiO$_2$ for photocatalytic methane halogenation is also evaluated by the recycling test, demonstrating the high photocatalytic stability of the system. The photocatalytic performance only shows a minor decrease after four cycles of reaction, which may result from slight loss of Cu element during cyclic test, and then becomes stable over the successive three cycles (Fig. 2e, Supplementary Fig. 22, Supplementary Tables 4, 5). Furthermore, we employ the KCl, MgCl$_2$ or seawater (containing water and rich NaCl), as chlorine sources. Surprisingly, such combinations of reactants can also allow the methane halogenation to proceed over Cu–TiO$_2$ (Fig. 2f), firmly implying the sustainability and low cost of this approach for photocatalytic methane halogenation. To further confirm the
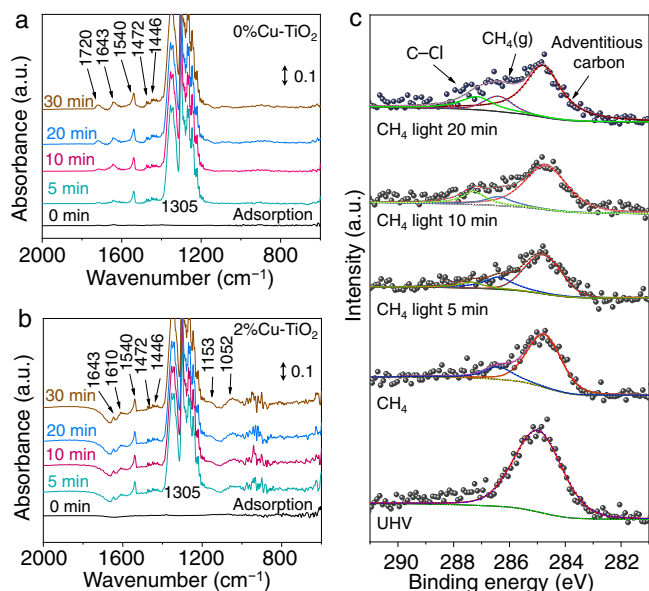
Fig. 3 | In situ characterization of photocatalytic CH₄ halogenation. a, b In situ DRIFTS spectra for photocatalytic methane halogenation over 0%Cu–TiO₂ (**a**) and 2%Cu–TiO₂ (**b**) using NaCl as halogenation agent under dark condition. **c** The C 1s region of AP-XPS spectra for 2%Cu–TiO₂ under different conditions.

universality of the photocatalytic methane halogenation, several sodium halides (i.e., NaF, NaCl and NaBr) are also applied for methane halogenation. As shown in Supplementary Fig. 23, the performance of methane halogenation using NaBr shows the highest methyl halide production rate (1.08 mmol h⁻¹ m⁻²), while the performance using NaF shows the lowest. These results suggest the universality of the photocatalytic methane halogenation and the strong correlation between halogenation efficiency and electronegativity of halogen. It is worth noting that, as compared with thermocatalytic methane halogenation using halogens or hydrogen halides, photocatalytic methane halogenation using alkali halides exhibits lower conversion and productivity (Supplementary Table 6). However, photocatalytic methane halogenation process can still find its specific application given the use of solar energy as power input and alkali halides as halogen source. For instance, offshore methane exploitation usually does not afford the power input for thermocatalytic conditions.

In situ characterization toward mechanism

To look into the reaction mechanism, we perform synchrotron-radiation-based in situ diffuse reflectance infrared Fourier-transform spectroscopy (DRIFTS) to monitor the reaction species evolution on the catalyst surface during the photocatalytic methane halogenation. Under dark condition (i.e., reactant adsorption), both 0%Cu–TiO₂ and 2%Cu–TiO₂ exhibit obvious peaks at ca. 1305, 1540 and 1446/1472 cm⁻¹ (Fig. 3a, b), assigned to the C–H deformation vibration of CH₄, C–H symmetric deformation vibrational mode of CH₄, and CH₃/CH₂ deformation vibrational modes, respectively[26–29]. Apart from these similarities, obvious differences can be observed on the DRIFTS spectra of 0%Cu–TiO₂ and 2%Cu–TiO₂. For 0%Cu–TiO₂, two peaks at ca. 1643 and 1720 cm⁻¹ assigned to C=O stretching vibration can be observed, demonstrating the formation of carboxylate species on the 0%Cu–TiO₂ surface[26,27,30]. These carboxylate species formed during reactant adsorption can be easily transformed into CO₂ during the photocatalytic methane halogenation reaction, collaborating the above-obtained photocatalytic methane halogenation results of 0% Cu–TiO₂, which is dominated with high CO₂ production selectivity[28,31,32]. In contrast, three additional peaks can be observed on the DRIFTS spectra of 2%Cu–TiO₂. At 1045 cm⁻¹, a peak attributed to hydroxyl groups (−OH) stretching can be observed, indicating that the

Cu can promote the transformation of adsorbed CH₄ into methyl species (−CH₃) and −OH, and suppress the formation of C=O and C–O species[33,34]. At 1153 and 1610 cm⁻¹, two peaks assigned to methoxy species (−OCH₃) are identified, implying that a small fraction of adsorbed methane is dissociated into −OCH₃[30,35]. When turning on the light, a peak at 715 cm⁻¹, assigned to C–Cl bond, can be observed and gradually grows over 2%Cu–TiO₂ upon light irradiation, further suggesting the generation of CH₃Cl from photocatalytic methane halogenation[36,37], while no significant changes can be observed for other species on the samples (Supplementary Fig. 24). These results manifest the essential role of Cu in dissociating methane molecules into hydroxyl and methyl species during the reactant adsorption on the catalyst surface.

As mentioned in the previous section, the Cu doping can cause the formation of oxygen vacancies on the Cu–TiO₂. To this end, the in situ electron paramagnetic resonance (EPR) spectroscopy measurements are performed to reveal the evolution of oxygen vacancies during the reaction. The EPR spectra collected under dark and light irradiation conditions in CH₄ atmosphere for 0%Cu–TiO₂ and 2%Cu–TiO₂ are shown in Supplementary Fig. 25. Under dark condition, both 0% Cu–TiO₂ and 2%Cu–TiO₂ exhibit obvious signals at $g = 2.00$ assigned to single electron-trapped surface defects (V_O^+ or O^-)[38,39], while 2% Cu–TiO₂ shows an additional broad characteristic Cu^{2+} signal at $g = 2.15$[25,40]. Upon light irradiation, the V_O^+ or O^- signal shows no detectable change for X%Cu–TiO₂. Meanwhile, the signal of Cu^{2+} for 2% Cu–TiO₂ distinctly decreases, revealing the reduction of Cu^{2+} into EPR-silent Cu^+ by photogenerated electrons[41]. Such a result suggests that the Cu dopant can accept the photogenerated electrons from the TiO₂ during the photocatalytic reaction, significantly enhancing the separation of photogenerated carriers.

To gain further insight into the photocatalytic methane halogenation pathway, the AP-XPS is performed to investigate the evolution of methane molecule and chlorine on the surface of 2%Cu–TiO₂ during the reaction (Supplementary Fig. 26)[42]. As shown in Fig. 3c, the C 1s AP-XPS spectrum collected in ultra-high vacuum (UHV) exhibits a peak at 284.8 eV, assigned to the adventitious carbon on the catalyst. Upon flowing CH₄ gas and H₂O vapor into the system, a new peak at 286.6 eV attributed to gaseous CH₄ appears. Upon light irradiation, a C 1s peak at 287.2 eV appears and gradually evolves, suggesting the stable formation of C–Cl bond[43–45]. For the Cl 2p AP-XPS spectrum, a typical NaCl peak can be found during the adsorption stage. Upon light irradiation, the Cl 2p spectrum becomes broader and slightly shifts toward higher binding energy (Supplementary Fig. 27), suggesting that the Cl ions of NaCl are oxidized by the photogenerated holes from 2% Cu–TiO₂. Such oxidized Cl species can subsequently couple with methyl groups (−CH₃), derived from dissociated methane, to form methyl chloride (CH₃Cl) under light irradiation, which is also confirmed by the slight shift of Cl 2p XPS peak toward higher binding energy as compared with NaCl (Supplementary Fig. 27).

Mechanism investigation

To further elucidate the reaction mechanism, the density functional theory (DFT) calculations are carried out to depict the energy profile of photocatalytic methane halogenation. We first calculate the dissociation energy of methane molecule on different photocatalysts. For the pristine TiO₂, although CH₄ molecule can be dissociated into *CH₃ with an electron energy change of 0.132 eV, the formed *CH₃ intermediates can hardly be stabilized (Supplementary Fig. 28). In contrast, the formed *CH₃ intermediates can be stabilized on the Cu–TiO₂ with the binding of their C and H atoms to Cu and O atoms of Cu–TiO₂, respectively (Fig. 4a). These results distinctly confirm that the role of Cu as intermediate stabilization sites during the dissociation of methane molecules. Based on the AP-XPS characterization, the Cl ions of NaCl are oxidized into *Cl intermediates by the photogenerated holes upon light irradiation. As such, the DFT calculations are
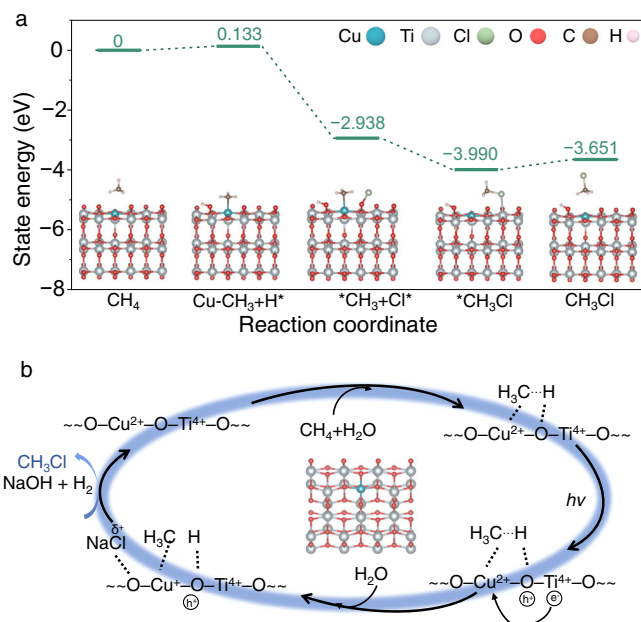
Fig. 4 | Proposed mechanism for photocatalytic CH₄ halogenation. a The DFT calculations for the production of CH₃Cl in photocatalytic methane halogenation on Cu-doped TiO₂. The insets show the optimized structures for each step. **b** The schematic illustration of the proposed mechanism for photocatalytic methane halogenation over Cu-doped TiO₂.

performed to examine the activation of Cl ions on the surface of Cu–TiO₂ catalyst under light irradiation. As shown in the Supplementary Fig. 29, the Cl ions from NaCl cluster on the surface of Cu–TiO₂ tend to lose the electrons and exhibit an oxidized state. Subsequently, these *Cl intermediates can couple with the stabilized *CH₃, forming *CH₃Cl with its C atom binding to Cu site with an electron energy change of −1.052 eV. Finally, the CH₃Cl molecules can be facilely desorbed from the surface of photocatalysts with a small energy change of 0.339 eV. Notably, the presence of H₂O can provide hydrogen source for H₂ production and oxygen source for regeneration of lattice oxygen. In detail, the H₂O can be first adsorbed on the oxygen vacancy, derived from the consumption of lattice oxygen during the generation of CH₃Cl and NaOH over Cu–TiO₂, which then is dissociated into OH* and (O)H* species neighboring the oxygen vacancy with an electron energy change of −1.498 eV (Supplementary Fig. 30). Upon irradiation, the H₂ can be formed and desorbed from the Cu–TiO₂ surface[46], while the oxygen from water will be filled into the lattice to regenerate the pristine structure of Cu–TiO₂. Given that the methoxy species are also resolved from the in situ DRIFTS characterization using Cu–TiO₂, the reaction route for photocatalytic methane halogenation based on methoxy species is also calculated. As shown in Supplementary Fig. 31, methane molecule can be easily dissociated into methoxy species (*O–CH₃) on the surface of Cu–TiO₂, which is exergonic with an electron energy change of −2.280 eV. However, the strong binding of the methoxy species (−5.059 eV) on the Cu–TiO₂ surface restricts them to proceed with the following transformations.

Taken together, in situ characterizations and DFT calculations indicate that the Cu dopants play a critical role for guiding the formation of the CH₃Cl during the photocatalytic methane halogenation. Specifically, during the reactant adsorption, the CH₄ molecules are first dissociated on the surface of Cu–TiO₂, forming methyl and hydroxyl species (Fig. 4b). These intermediate species can subsequently be stabilized by the Cu and TiO₂. Upon light irradiation, the photogenerated holes on the Cu–TiO₂ can oxidize the NaCl to form active halogen species, which can couple with methyl to form methyl

chloride; simultaneously, the photogenerated electrons transferred from TiO₂ to Cu can be utilized for reducing the H to produce H₂.

Discussion

Methyl halide, a highly versatile platform molecule, can be facilely transformed into value-added chemicals (e.g., fuels, pharmaceutical intermediates and organoboron agents) under relatively mild conditions (Supplementary Table 7)[14,23]. To show the high feasibility of our strategy, we construct a cycling reaction system for photocatalytic methane conversion into methanol via a methyl chloride mediated pathway. As shown in Supplementary Fig. 32, methyl chloride is first obtained through photocatalytic methane halogenation. Subsequently, methyl chloride can be directly mixed with the NaOH aqueous solution, forming methanol. As an outcome, methanol can be produced with a production rate of 0.51 mmol h⁻¹ m⁻² via the constructed methane conversion system at 80 °C (Supplementary Fig. 33). It should be noted here that the H₂ and NaCl are the only two byproducts of the overall reaction. The H₂ can be used as the fuels, while the NaCl can be recycled into the reaction system for sustaining the overall reaction (Supplementary Fig. 32). Given that no any contaminated feedstock or byproducts can be found in such a reaction system, it is a green and sustainable methane conversion approach.

Apart from fuel production, methyl halide can be also applied for synthesizing high-value pharmaceutical intermediates at mild conditions. To further show the multi-purpose features of methyl halide in chemical manufacturing, we demonstrate the synthesis of methyl o-toluate and 1-methylindole (Entry 2 and 3 in Supplementary Table 7) which are essential intermediates for anti-cancer drugs, using methyl halide as precursors. As shown in Supplementary Figs. 34–37, high selectivity toward methyl o-toluate and 1-methylindole can be obtained under mild conditions (0 °C– room temperature) in N,N-dimethylformamide solution over CH₃Br.

In summary, we present a selective and sustainable photocatalytic methane halogenation strategy for methyl halide production using cost-effective and noncorrosive NaCl over Cu-doped porous TiO₂ nanostructures. In details, a methyl chloride production rate of 0.61 mmol h⁻¹ m⁻² and a methyl bromide production rate of 1.08 mmol h⁻¹ m⁻² are achieved using optimized Cu–TiO₂ at room temperature and ambient pressure. On the basis of in situ characterization techniques and theoretical calculation, it is confirmed that the Cu plays a critical role in such a reaction, where it can be utilized to stabilize the *CH₃ for its coupling with Cl⁻ to form the targeted CH₃Cl. This work presents a fresh perspective for photocatalytic activation of alkali halides toward methane halogenation under mild conditions, and paves the way for efficient methane conversion into value-added chemicals as well as offshore methane exploitation through a highly sustainable approach.

Methods
Material synthesis
The Cu-doped porous TiO₂ nanostructures (X%Cu–TiO₂) were synthesized through a sol-gel method. In a typical synthesis, 2.4 g F127 was dissolved in 30 mL ethanol under stirring. Then 3.4 mL Ti(OBu)₄, a specific amount of Cu(NO₃)₂·3H₂O, 2.3 mL acetic acid and 2.0 mL hydrochloric acid were added into the F127 solution. The mixture was stirred vigorously for 2 h and transferred into a petri dish (diameter 125 mm), and heated on a hotplate at 40 °C for 12 h. After evaporation of ethanol, a transparent gel was formed, and was transferred into a 65 °C oven for additional 24 h aging. Finally, the gel was calcined at 450 °C in the air for 5 h with a ramp rate of 2 °C min⁻¹ to obtain Cu-doped porous TiO₂ nanostructures. The Cu-doped porous TiO₂ samples were denoted as X%Cu–TiO₂, where X was the molar percentage of the doped Cu element. The porous TiO₂ (TiO₂) was synthesized by following the same procedure except for the absence of Cu(NO₃)₂·3H₂O.

XAS characterization

Synchrotron-radiation-based O K-edge, Ti L-edge and Cu L-edge XAS measurements were carried out at the MCD-A and MCD-B beamlines (Soochow Beamline for Energy Materials) (BL12B) of National Synchrotron Radiation Laboratory (NSRL) in Hefei, China. The electron beam energy of the storage ring was 800 MeV with an average stored current of 300 mA. The photo energy ranged from 100 to 1000 eV with an energy resolution of 0.2 eV. All of the data were recorded in the total electron yield (TEY) mode by collecting the sample drain current under a vacuum greater than 5×10^{-8} Pa. The resolving power of the grating was typically $E/\Delta E = 1000$, and the photon flux was 5×10^{8} photons per second. The XAS spectra of standard anatase TiO_2, Cu_2O and CuO powders were collected for comparison. Ti K-edge and Cu K-edge XAS measurements were performed at the beamline 1W1B of Beijing Synchrotron Radiation Facility (BSRF) in Beijing, China. The storage ring of BSRF was operated at 2.5 GeV with the maximum stored current of 250 mA.

SRPES characterization

SRPES experiments were performed at the Photoemission Endstation (BL10B) in the NSRL. Valence-band spectra were measured using synchrotron-radiation light as the excitation source with a photon energy of 169.50 eV and referenced to the Fermi level ($E_F = 0$) determined from Au. A sample bias of −10 V was applied in order to observe the secondary electron cutoff. The work function (Φ) was determined by the difference between the photon energy and the width of whole valence-band spectra.

In situ DRIFTS characterization

In situ DRIFTS measurements were performed using a Bruker IFS 66v Fourier-transform spectrometer equipped with a Harrick diffuse reflectance accessory at the Infrared Spectroscopy and Microspectroscopy Endstation (BL01B) of NSRL. Each spectrum was recorded by averaging 256 scans at a resolution of 4 cm^{-1}. The samples were placed in an infrared (IR) reaction chamber sealed with ZnSe windows, which is specifically designed to examine highly scattered powder samples in diffuse reflection mode. After sample loading, the chamber was purged with argon gas (99.999%) for 30 min. Then the spectrum was collected as background spectrum. During the in situ characterization, pure CH_4 gas (99.999%) was continually introduced into the chamber.

Photocatalytic methane halogenation

Photocatalytic methane halogenation experiments were performed in CH_4 atmosphere at room temperature using sodium chloride as halogenation agent. Typically, 100 mg sample and specific amounts of NaCl (e.g., 10 mg, 20 mg) were dispersed in 5 mL water in a home-made quartz reactor with a diameter of 6 cm. The sample was sonicated for 5 min to form a uniform suspension and transferred in an oven at 80 °C for 5 h. After drying, 100 μL water was dropped into the notch on the reactor. The reactor was purged with CH_4 (99.999%) for 30 min and sealed with rubber seals. Then the reactor was irradiated by a 300 W xenon lamp (PLS-SXE300, Perfect light) with a lighting area of 28.26 cm^2. After irradiation for 4 h, the reacted gas was detected by gas chromatography (GC, 7890B, Ar carrier, Agilent) equipped with a methanation reactor (i.e., a nickel catalyst tube), a flame ionization detector (FID) and a thermal conductivity detector (TCD) for the determination of methane halides, hydrocarbons, H_2, CO and CO_2.

Computational method

Spin-polarized calculations were performed with density functional theory (DFT) methods implemented in Vienna ab initio simulation package (VASP)[47,48]. Perdew, Burke and Ernzerhof (PBE)[49] for the exchange–correlation functional of generalized gradient approximation and a plane wave cutoff of 500 eV were used. The Grimme's DFT-D3 scheme[50] was adopted to describe the long-range Van der Waals (vdW)

interactions. In the structural optimizations, a limited number of top layers were allowed to relax with the conjugate gradient method until the residual forces were less than 0.03 eV Å^{-1}. The energy convergence was 10^{-5} eV. The tetragonal anatase titanium dioxide (TiO_2) bulk lattice parameters used in all calculations were $a = b = 3.817$, c = 9.575 Å and $\alpha = 90°$, $\beta = 90°$, $\gamma = 90°$ according to experimental results. A slab model containing $1 \times 3 \times 1$ unit cells of anatase (101) surface was adopted to simulate key intermediates adsorption behaviors on anatase surface. The thickness of vacuum layer was 20 Å in a direction perpendicular to the surface to avoid the interaction between two neighboring slabs. The first Brillouin zone was sampled with $1 \times 1 \times 1$ k-points both for structure optimization. The adsorption energy of CH$_4$* (E_{ads}) was calculated based on the following formulas: $E_{ads}(CH_4*) = E(CH_4*) − E(*) − E(CH_4)$. $E(*)$ and $E(CH_4*)$ were the total energies of anatase(101) surface or Cu(copper) doped anatase(101) surface, and CH$_4$* adsorbed surface.

Reporting summary

Further information on research design is available in the Nature Portfolio Reporting Summary linked to this article.

Data availability

All data that support the findings in this paper are available within the article and its Supplementary Information or are available from the corresponding authors upon reasonable request. Source data for the following figures are provided with this paper. Figures 2a–f, 3a–c, Extended Data Fig. 1e–g, Fig. S3a–e, Fig. S4, Fig. S5, Fig. S6a, b, Fig. S7, Fig. S9a, b, Fig. S10a–c, Fig. S11a, b, Fig. S13, Fig. S14a, b, Fig. S15a, b, Fig. S16a, b, Fig. S17a, b, Fig. S18, Fig. S19, Fig. S20a, b, Fig. S21d–f, Fig. S22, Fig. S23a, b, Fig. S24a, b, Fig. S26, Fig. S32, Fig. S32, Fig. S33, Fig. S34, Fig. S35, Fig. S36. Source data are provided with this paper.

References

1. Lin, R., Amrute, A. P. & Pérez-Ramírez, J. Halogen-mediated conversion of hydrocarbons to commodities. *Chem. Rev.* **117**, 4182–4247 (2017).
2. Kim, Y. et al. Sulfated tin oxide as highly selective catalyst for the chlorination of methane to methyl chloride. *ACS Catal.* **9**, 9398–9410 (2019).
3. McFarland, E. Unconventional chemistry for unconventional natural gas. *Science* **338**, 340–342 (2012).
4. Fang, X. et al. Highly enhanced aromatics selectivity by coupling of chloromethane and carbon monoxide over H-ZSM-5. *Angew. Chem. Int. Ed.* **61**, e202114953 (2022).
5. Schmidt, S. A. et al. Preparation and characterization of neat and $ZnCl_2$ modified zeolites and alumina for methyl chloride synthesis. *Appl. Catal. A* **468**, 120–134 (2013).
6. Terlingen, B. et al. Mechanistic insights into the lanthanide-catalyzed oxychlorination of methane as revealed by operando spectroscopy. *ACS Catal.* **11**, 10574–10588 (2021).
7. Fan, Y. et al. Selective photocatalytic oxidation of methane by quantum-sized bismuth vanadate. *Nat. Sustain.* **4**, 509–515 (2021).
8. Ma, J. et al. Efficient photoelectrochemical conversion of methane into ethylene glycol by WO_3 nanobar arrays. *Angew. Chem. Int. Ed.* **60**, 9357–9361 (2021).
9. Ma, J., Long, R., Liu, D., Low, J. & Xiong, Y. Defect engineering in photocatalytic methane conversion. *Small Struct.* **3**, 2100147 (2022).
10. Low, J., Ma, J., Wan, J., Jiang, W. & Xiong, Y. Identification and design of active sites on photocatalysts for the direct artificial carbon cycle. *Acc. Mater. Res.* **3**, 331–342 (2022).
11. Luo, L. et al. Synergy of Pd atoms and oxygen vacancies on In_2O_3 for methane conversion under visible light. *Nat. Commun.* **13**, 2930 (2022).
12. Zheng, K. et al. Room-temperature photooxidation of CH_4 to CH_3OH with nearly 100% selectivity over hetero-ZnO/Fe_2O_3 porous nanosheets. *J. Am. Chem. Soc.* **144**, 12357–12366 (2022).

13. Olah, G. A. et al. Electrophilic reactions at single bonds. 20. Selective monohalogenation of methane over supported acidic or platinum metal catalysts and hydrolysis of methyl halides over γ-alumina-supported metal oxide/hydroxide catalysts. A feasible path for the oxidative conversion of methane into methyl alcohol/dimethyl ether. *J. Am. Chem. Soc.* **107**, 7097–7105 (1985).

14. Taifan, W. & Baltrusaitis, J. CH_4 conversion to value added products: Potential, limitations and extensions of a single step heterogeneous catalysis. *Appl. Catal. B* **198**, 525–547 (2016).

15. Batamack, P. T. D., Mathew, T. & Prakash, G. K. S. One-pot conversion of methane to light olefins or higher hydrocarbons through H-SAPO-34-catalyzed in situ halogenation. *J. Am. Chem. Soc.* **139**, 18078–18083 (2017).

16. Zichittella, G., Paunović, V., Amrute, A. P. & Pérez-Ramírez, J. Catalytic oxychlorination versus oxybromination for methane functionalization. *ACS Catal.* **7**, 1805–1817 (2017).

17. Li, D. et al. Photocatalytic chlorination of methane using alkali chloride solution. *ACS Catal.* **12**, 7004–7013 (2022).

18. Lin, R. et al. Efficient and stable silica-supported iron phosphate catalysts for oxidative bromination of methane. *J. Catal.* **272**, 65–73 (2010).

19. Ogura, K. & Takamagari, K. Direct conversion of methane to methanol, chloromethane and dichloromethane at room temperature. *Nature* **319**, 308–308 (1986).

20. Ogura, K. & Emura, N. Selective photochemical monochlorination of methane. *J. Mol. Catal.* **45**, 319–325 (1988).

21. Hirscher, N. A. et al. A metal-free, photocatalytic method for aerobic alkane iodination. *J. Am. Chem. Soc.* **143**, 19262–19267 (2021).

22. Paunović, V., Zichittella, G., Moser, M., Amrute, A. P. & Pérez-Ramírez, J. Catalyst design for natural-gas upgrading through oxybromination chemistry. *Nat. Chem.* **8**, 803–809 (2016).

23. Bilke, M., Losch, P., Vozniuk, O., Bodach, A. & Schüth, F. Methane to chloromethane by mechanochemical activation: a selective radical pathway. *J. Am. Chem. Soc.* **141**, 11212–11218 (2019).

24. Zhao, Y. et al. Tuning oxygen vacancies in ultrathin TiO_2 nanosheets to boost photocatalytic nitrogen fixation up to 700 nm. *Adv. Mater.* **31**, 1806482 (2019).

25. Lee, B.-H. et al. Reversible and cooperative photoactivation of single-atom Cu/TiO_2 photocatalysts. *Nat. Mater.* **18**, 620–626 (2019).

26. Zhang, R. et al. Photocatalytic oxidative dehydrogenation of ethane using CO_2 as a soft oxidant over Pd/TiO_2 catalysts to C_2H_4 and syngas. *ACS Catal.* **8**, 9280–9286 (2018).

27. Yee, A., Morrison, S. J. & Idriss, H. A study of the reactions of ethanol on CeO_2 and Pd/CeO_2 by steady state reactions, temperature programmed desorption, and in situ FT-IR. *J. Catal.* **186**, 279–295 (1999).

28. Chen, X. et al. Photocatalytic oxidation of methane over silver decorated zinc oxide nanocatalysts. *Nat. Commun.* **7**, 12273 (2016).

29. Li, C. & Xin, Q. FT-IR spectroscopic investigation of methane adsorption on cerium oxide. *J. Phys. Chem.* **96**, 7714–7718 (1992).

30. Jung, K. T. & Bell, A. T. An in situ infrared study of dimethyl carbonate synthesis from carbon dioxide and methanol over zirconia. *J. Catal.* **204**, 339–347 (2001).

31. Tao, F. F. et al. Understanding complete oxidation of methane on spinel oxides at a molecular level. *Nat. Commun.* **6**, 7798 (2015).

32. Yang, C.-C., Yu, Y.-H., van der Linden, B., Wu, J. C. S. & Mul, G. Artificial photosynthesis over crystalline TiO_2-based catalysts: Fact or fiction? *J. Am. Chem. Soc.* **132**, 8398–8406 (2010).

33. Lavalley, J. C. et al. FT-IR study of the δ(OH) mode of surface hydroxy groups on metal oxides. *J. Mol. Struct.* **175**, 453–458 (1988).

34. Ermini, V., Finocchio, E., Sechi, S., Busca, G. & Rossini, S. An FT-IR and flow reactor study of the conversion of propane on γ-Al_2O_3 in oxygen-containing atmosphere. *Appl. Catal. A* **190**, 157–167 (2000).

35. Kähler, K., Holz, M. C., Rohe, M., Strunk, J. & Muhler, M. Probing the reactivity of ZnO and Au/ZnO nanoparticles by methanol adsorption: A TPD and DRIFTS study. *ChemPhysChem* **11**, 2521–2529 (2010).

36. Stoyanov, E. S., Stoyanova, I. V., Tham, F. S. & Reed, C. A. Dialkyl chloronium ions. *J. Am. Chem. Soc.* **132**, 4062–4063 (2010).

37. Mo, A. K. et al. Understanding the mechanism of solvent-mediated adhesion of vacuum deposited Au and Pt thin films onto PMMA substrates. *Adv. Funct. Mater.* **23**, 1431–1439 (2013).

38. Coronado, J. M. et al. EPR study of the surface characteristics of nanostructured TiO_2 under UV irradiation. *Langmuir* **17**, 5368–5374 (2001).

39. Zhang, Z. et al. Probing the electronic structure and photoactivation process of nitrogen-doped TiO_2 using DRS, PL, and EPR. *ChemPhysChem* **13**, 1542–1550 (2012).

40. Docao, S. et al. Solar photochemical–thermal water splitting at 140 °C with Cu-loaded TiO_2. *Energy Environ. Sci.* **10**, 628–640 (2017).

41. Jiang, W. et al. Pd-modified ZnO–Au enabling alkoxy intermediates formation and dehydrogenation for photocatalytic conversion of methane to ethylene. *J. Am. Chem. Soc.* **143**, 269–278 (2021).

42. Cai, J. et al. An APXPS endstation for gas–solid and liquid–solid interface studies at SSRF. *Nucl. Sci. Tech.* **30**, 81 (2019).

43. Moulder, J. F., Stickle, W. F., Sobol, W. M. & Bomben, K. D. *Handbook of X-Ray Photoelectron Spectroscopy* (Perkin-Elmer Corporation, 1992).

44. Pérez-Cadenas, A. N. F., Maldonado-Hódar, F. J. & Moreno-Castilla, C. On the nature of surface acid sites of chlorinated activated carbons. *Carbon* **41**, 473–478 (2003).

45. Chang, H. P. & Thomas, J. H. An XPS study of X-ray-induced dehydrochlorination of oxygen-free PVC. *J. Electron Spectrosc.* **26**, 203–212 (1982).

46. Silva, L. A., Ryu, S. Y., Choi, J., Choi, W. & Hoffmann, M. R. Photocatalytic hydrogen production with visible light over Pt-interlinked hybrid composites of cubic-phase and hexagonal-phase CdS. *J. Phys. Chem. C* **112**, 12069–12073 (2008).

47. Kresse, G. & Hafner, J. Ab initio molecular dynamics for liquid metals. *Phys. Rev. B* **47**, 558–561 (1993).

48. Kresse, G. & Furthmüller, J. Efficient iterative schemes for ab initio total-energy calculations using a plane-wave basis set. *Phys. Rev. B* **54**, 11169–11186 (1996).

49. Perdew, J. P., Burke, K. & Ernzerhof, M. Generalized gradient approximation made simple. *Phys. Rev. Lett.* **77**, 3865–3868 (1996).

50. Grimme, S., Antony, J., Ehrlich, S. & Krieg, H. A consistent and accurate ab initio parametrization of density functional dispersion correction (DFT-D) for the 94 elements H-Pu. *J. Chem. Phys.* **132**, 154104 (2010).

Acknowledgements

Author contributions

R.L. and Y.X. supervised the project. J.M. R.L. and Y.X. conceived and designed the experiments. J.M. performed the key experiments and analyzed the results. W.J., J.L., Z.Q., Y.Z., H.Z., and Z.L. assisted to carry out the in situ EPR, DRIFTS and AP-XPS characterization. D.D., H.J., D.L., S.C., and L.S. assisted to perform the XAS characterization. K.M. performed the materials simulations. C.Z. and K.W. assisted to perform the synthesis of methyl o-toluate and 1-methylindole. J.M., J.L, R.L., and Y.X. co-wrote the manuscript. All the authors discussed the results and commented on the manuscript.

Competing interests

A patent application was authorized by China National Intellectual Property Administration (patentee: University of Science and Technology of China; names of inventors: Yujie Xiong, Jun Ma, Ran Long; patent number: ZL202011083083.7; status of application: authorized; specific aspect of manuscript covered in the patent application: the photocatalytic method for generation of methyl halide using alkali halides). The remaining authors declare no competing interests.

Additional information

Supplementary information The online version contains supplementary material available at https://doi.org/10.1038/s41467-023-36977-0.

Correspondence and requests for materials should be addressed to Ran Long or Yujie Xiong.

Peer review information *Nature Communications* thanks Zizhong Zhang and the other, anonymous, reviewers for their contribution to the peer review of this work.

Reprints and permissions information is available at http://www.nature.com/reprints

Publisher's note Springer Nature remains neutral with regard to jurisdictional claims in published maps and institutional affiliations.